Micro-patterned molecularly imprinted polymer structures on functionalized diamond-coated substrates for testosterone detection

Peer-reviewed author version

KELLENS, Evelien; BOVE, Hannelore; VANDENRYT, Thijs; LAMBRICHTS, Jeroen; Dekens, Jolien; DRIJKONINGEN, Sien; D'HAEN, Jan; DE CEUNINCK, Ward; THOELEN, Ronald; JUNKERS, Tanja; HAENEN, Ken & ETHIRAJAN, Anitha (2018)
Micro-patterned molecularly imprinted polymer structures on functionalized diamond-coated substrates for testosterone detection. In: BIOSENSORS & BIOELECTRONICS, 118, p. 58-65.

DOI: 10.1016/j.bios.2018.07.032
Handle: http://hdl.handle.net/1942/27697

Article type: Full Paper

Micro-Patterned Molecularly Imprinted Polymer Structures on Functionalized Diamond-Coated Substrates for Testosterone Detection

Evelien Kellens[a§], Hannelore Bové[a§], Thijs Vandenryt[a], Jeroen Lambrichts[a], Jolien Dekens[a], Sien Drijkoningen[a,b], Jan D'Haen[a,b], Ward De Ceuninck[a,b], Ronald Thoelen[a,b], Tanja Junkers[a,1], Ken Haenen[a,b] and Anitha Ethirajan[a,b]*

[§] Both authors contributed equally to this work

* Corresponding author: anitha.ethirajan@uhasselt.be

[a] Institute for Materials Research (IMO), Hasselt University, Wetenschapspark 1 and Agoralaan D, 3590 Diepenbeek, Belgium

[b] IMOMEC, IMEC vzw, Wetenschapspark 1, 3590 Diepenbeek, Belgium

[1] Present address: School of Chemistry, 19 Rainforest Walk, Monash University Clayton, VIC 3800, Australia

Abstract

Molecularly imprinted polymers (MIPs) can selectively bind target molecules and can therefore be advantageously used as a low-cost and robust alternative to replace fragile and expensive natural receptors. Yet, one major challenge in using MIPs for sensor development is the lack of simple and cost-effective techniques that allow firm fixation as well as controllable and consistent receptor material distribution on the sensor substrate. In this work, a convenient method is presented wherein microfluidic systems in conjunction with in situ photo-polymerization on functionalized diamond substrates are used. This novel strategy is simple, efficient, low-cost and less time consuming. Moreover, the approach ensures a tunable and consistent MIP material amount and distribution between different sensor substrates and thus a controllable active sensing surface. The obtained patterned MIP structures are successfully tested as a selective sensor platform to detect physiological concentrations of the hormone disruptor testosterone in buffer, urine and saliva using electrochemical impedance spectroscopy. The highest added testosterone concentration (500 nM) in buffer resulted in an impedance signal of 10.03 ± 0.19 % and the lowest concentration (0.5 nM) led to a measurable signal of 1.8 ± 0.15 % for the MIPs. With a detection limit of 0.5 nM, the MIP signals exhibited good linearity between 0.5 nM to 20 nM concentration range. Apart from the excellent and selective recognition offered by these MIP structures, they are also stable during and after the dynamic sensor measurements. Additionally, the MIPs can be easily regenerated by a simple washing procedure and are successfully tested for their reusability.

Keywords: microfluidics, molecularly imprinted polymers, biosensors and body fluids

1 Introduction

The demand for the detection and quantification of molecules in the fields of molecular screening, clinical diagnostics, and food- and environmental analysis is growing fast. Often, target molecule quantification in samples is performed in laboratories using analysis techniques such as immuno-assays, gas and liquid chromatography (or others), which are time consuming, laborious, costly and require stringent conditions and specialized personnel (Fitzgerald et al. 2010; Vera et al. 2011; Wang et al. 2014; Wild 2013). Therefore, interest in the development of cheaper, reusable, faster and more user-friendly sensors is increasing. Typically, recognition elements that are capable of binding target molecules are immobilized on a signal transducer substrate in these sensors. The binding events can be translated *via* electronic or optical read-out techniques into a concentration-dependent signal (Chen et al. 2016; Liu et al. 2018; Yang et al. 2018a). Biological macromolecules such as antibodies, enzymes, and cells are commonly used as recognition elements since they possess highly fine-tuned and effective molecular recognition (Eersels et al. 2013; Gooding 2002; Liss et al. 2002; Wang 2001). However, typically these natural receptors are on the one hand costly and laborious to obtain, and on the other hand they exhibit physical and chemical instability as well as insufficient sensitivity in non-physiological environments (Ruigrok et al. 2011). A compelling alternative is the use of so-called synthetic biomimetic receptors, which are highly stable and cost-effective. In this regard, the use of molecularly imprinted polymers (MIPs) has tremendous potential to be used as artificial receptors for biosensing applications (Piletsky et al. 2001; Sellergren 2000; Whitcombe and Vulfson 2001). In general, MIPs are obtained when the target/template molecule is present in the matrix during polymerization. The functional groups of the monomer are arranged around the template molecule through non-covalent or covalent interactions. After polymerization, the subsequent removal of the template leaves nano-cavities (**Figure 1A**). These cavities are complementary to the template in terms of size, shape, and arrangement of the functional groups, allowing these polymer

imprints to rebind the target molecule with high affinity and specificity (Peeters et al. 2012). In contrast with natural receptors, these artificial receptors allow for a long shelf-time storage as well as chemical and physical robustness, even in extreme pH-environments (Piletsky et al. 2001; Sellergren and Allender 2005).

The geometries of MIPs can be chosen depending on the requirements of the application. For sensor applications, MIPs have been used in the form of *ex situ* prepared particles which were subsequently immobilized on the sensor substrate (Kamra et al. 2015; Peeters et al. 2013; Wackers et al. 2014) but also in the form of films or structures which are directly in situ polymerized and grafted on the sensor substrate (Chen et al. 2015; Fuchs et al. 2013). Recently, simultaneous wet phase inversion and imprinting was used to obtain MIP films on electrode surfaces, where the sensor performance as a function of the film thickness was studied (Yang et al. 2018b). Frequently used sensor read-out techniques, which quantify the binding between the target molecule and MIP based sensing electrodes, include impedance spectroscopy (Betatache et al. 2014), quartz crystal microbalance (Reimhult et al. 2008) and surface plasmon resonance (Tan et al. 2015).

MIPs in the form of *ex situ* prepared particles are very interesting for sensor applications due to their high and controllable active sensing surface. Bulk polymerization with subsequent grinding is an established and widely used method as it is a fast and simple method to produce MIPs. As the bulk monoliths after mechanical grinding results in micron-sized particles with irregular shapes and sizes (Alexander et al. 2006; Svenson and Nicholls 2001), the applicability of these particles on sensor substrates is of concern. It is of most importance that the detection of a target molecule in a sample is reliable and consistent. Therefore, all inhomogeneities between different transducer substrates need to be reduced to a minimum. To obtain more control over the shape, particle size and surface area of the MIPs, colloidal MIP synthesis methods such as precipitation (Yang et al. 2010), suspension (Pérez-Moral and Mayes 2004), and emulsion (Vaihinger et al. 2002) techniques are compelling alternatives.

Issues which still need to be overcome are stable MIP attachment to the substrate (even in dynamic conditions) and consistency in amount and distribution of the polymer in and between different sensor substrates. Therefore, there has been a tremendous focus on techniques that allow to create stable and reliable sensing substrates in a reproducible way. MIP particles have been previously deposited using methods such as stamping, screen-printing, drop casting and spin coating (Chianella et al. 2003; Lavine et al. 2007; Wackers et al. 2014). In general, reliable MIP attachment, a consistent material amount and distribution on the substrate are important issues for sensor measurements. However, with these deposition techniques one or a combination of these issues still exist. With stamping procedures, substrates with an adhesive layer are used and the particles are pressed on to the adhesive polymer using a stamp. As the MIP is partially embedded into the adhesive layer, not the entire MIP particle is available for recognition purposes. In addition, partial embedding might likely cause problems if the particles come loose during the measurement. Moreover, if bulk MIP particles in the form of dried powder are stamped it is difficult to control the material amount and distribution on the adhesive layer. In case of screen printing, additional additives are needed which might block the MIP surface or interfere with the recognition ability of the MIP, depending on the choice of the additives used. Furthermore, when drop casting or spin coating approaches are employed, dispersions of particles in suitable solvents without aggregates are needed. Additionally, the dilution of the dispersion has to be optimal in order to have a good coverage on the substrate without aggregate formation. It is also crucial that the coated MIP particles on the substrate need to be firmly attached to the substrate in order to avoid problems during the sensor measurements. In this regard, particles have been immobilized on the biosensor substrate through linker molecules or by the use of an aforementioned adhesive polymer layer (Alenus et al. 2012; Kamra et al. 2015; Peeters et al. 2012). Although these immobilization methods have proven their applicability, a stable coupling between the MIP particle and the substrate which is strong

enough to endure the dynamic sensor measurement conditions and ensure sensor regeneration for reusability remains challenging. In addition, many problems are still existing to find a technique that allows control over the MIP particle amount and distribution on the sensor substrate. Alternatively, homogeneous MIP films are also deposited on the substrates. However, depending on the thickness of the film, the removal of the template molecules might pose a problem due to the reduced surface area.

A major advance in the field was the direct *in situ* coupling and patterning of MIPs on the sensor surface. In this way, identical amounts and geometries of imprinted polymer can be achieved to act as molecular recognition layer. Previously, photolithographic methods (Acikgoz et al. 2011; Boysen et al. 2014) and advanced fabrication techniques such as scanning-beam, projection, and interference (holography) photography (Fuchs et al. 2013; Gates et al. 2004; Linares et al. 2011) have been reported. Also, non-optical based approaches including electrodeposition (Tretjakov et al. 2016), self-assembly (Apodaca et al. 2011), and microfluidic molds (Choi 2014) or stencils (Ayela et al. 2014) have been used. However, major problems associated with in situ patterning techniques are multi-step and time-consuming procedures and the use of expensive equipment. Therefore, it is highly desired to have a low-cost and time-efficient method which ensures on the one hand that every time identical amounts of pre-polymerization precursor mixture are polymerized in identical geometries with a high active sensing surface, and on the other hand an extremely firm attachment of the latter on the sensor substrate. The high surface area allows for reducing the total washing time to remove the template molecules to a minimum, which leads to a faster regeneration of the substrate. The bond between the MIP material and the sensor substrate should be strong enough so that no polymer detaches during the sensor measurements. This ensures the reliability of the sensor detection results and allows for successful reusability of the sensor substrate.

In this work, we report a simple and elegant fabrication of patterned MIP structures with geometries defined by the microfluidic stamp and the reliable attachment to the diamond electrode surface for the convenient detection of physiological concentrations of testosterone in samples comprising of real biological fluids using an impedimetric set-up under dynamic flow conditions (**Figure 1B**). Electrochemical impedance spectroscopy (EIS) was used as an electronic read out technique as it is sensitive, simple to use, inexpensive, fast, offers miniaturization possibilities, and integration with other techniques if needed. A boron-doped bio-inert nano-crystalline diamond (NCD) layer deposited on a highly doped silicon wafer was used as a substrate/electrode material. The conductive NCD was used as sensor interface for biological applications because of the materials' unique properties, namely the large electrochemical potential window, chemical inertness, physicochemical stability and biocompatibility (Bakowicz-Mitura et al. 2007; Grieten et al. 2011; Rubio-Retama et al. 2006; Vermeeren et al. 2011; Wenmackers et al. 2009). Due to its poor chemical stability, bare silicon substrates are prone to the formation of a silicon oxide layer, which would cause a drift in the impedance signal due to increasing capacitive effects. Various approaches to immobilize (bio-) molecules on diamond thin films have already been investigated (Hartl et al. 2004; Hernando et al. 2007; Yang et al. 2002) and have also been successfully tested further for impedimetric sensing (van Grinsven et al. 2011). In this work, molecularly imprinted polymer structures were immobilized on diamond substrates by means of a simple and efficient carbon coating step combined with microfluidic molds. This approach allows for obtaining MIP structures with a controlled morphology. Jordan and co-workers have successfully demonstrated carbon templating on diamond substrates for grafting polymer chains and biofunctionalization (Hutter et al. 2011; Steenackers et al. 2009). Although a high spatial resolution and a small size range can be achieved, the drawback of the previously used method for carbon templating is that for every sensor substrate electron beam (e-beam) lithography needs to be performed, which is expensive and laborious. Therefore, in here the

184 focus is laid on reducing the multi-step and time consuming synthesis procedures by using a
185 simple and fast carbon coating step to deposit a stable thin layer (20 nm) of amorphous
186 carbonaceous material over the whole transducer interface. The reactive bonds of the
187 amorphous carbon allow ultraviolet (UV)-induced photografting and covalent attachment of
188 polymer structures across the entire sensor surface. To structure the polymer into patterned
189 MIP structures with effective transducer surface coverage and defined dimensions, the
190 monomer-target molecule precursor mixture is deposited on the substrate by using a patterned
191 elastic polydimethylsiloxane (PDMS) based microfluidic flow cell. To obtain this PDMS flow
192 cell, first a master structure is created using e-beam lithography. Subsequently, from this
193 master structure, numerous PDMS molds can be obtained using the master as a cast. As a
194 proof of concept, MIP structures for testosterone detection were targeted. Testosterone is a
195 steroid hormone disruptor and concentrations deviating from the physiological concentrations
196 are associated with several health conditions (Thieme and Hemmersbach 2009), like breast
197 cancer in women (Cauley et al. 1999) as well as prostate and lung cancer in men (Hyde et al.
198 2012). A bi-functional crosslinking monomer – N,O-bismethacryloyl ethanolamine (NOBE)
199 (LeJeune and Spivak 2007) – was used as we have shown previously that NOBE is a very
200 suitable monomer for the non-covalent imprinting of testosterone (Kellens et al. 2016). It is
201 worth to note that by using a bi-functional monomer the need for additional functional
202 monomers and empirical optimization of the relative ratios in the formulation is eliminated.
203 After the photografting and in situ polymerization of the monomer-target molecule precursor
204 mix, the template molecules were removed from the imprints by washing steps. The emptied
205 cavities are then available for rebinding of the template molecule with high affinity and
206 specificity.

207 The use of microfluidic systems in combination with MIPs is already described in
208 literature (Birnbaumer et al. 2009; Choi 2014; Weng et al. 2007). However, the combination
209 of micropatterned MIP structures and reliable immobilization on an electrochemically inert

NCD sensor substrate using a coordinated sequence of simple surface treatment steps (hydrogen termination followed by thin carbon layer deposition) for selective impedimetric sensing of target molecules has to the best of our knowledge not been reported yet in literature. For every sensor measurement, a non-imprinted polymer (NIP) structure with identical geometries was used. This negative control was synthesized and handled in the same way as the MIP but in the absence of the template molecules during polymerization. To test the selectivity of the MIP structures for the target molecule, the binding characteristics towards molecules that are structurally similar to testosterone, such as estriol and *β*-estradiol, are tested (**Figure 1C**).

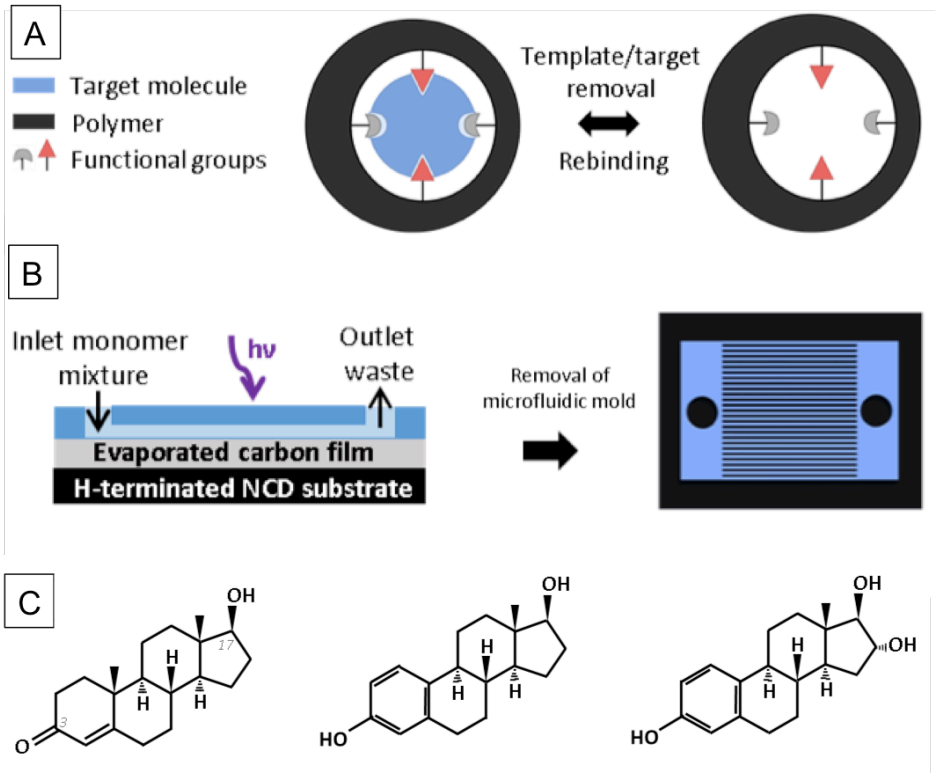

Figure 1: (A) Scheme showing the principle to obtain molecularly imprinted polymers. (B) Schematic representation of the method to reliably obtain microstructured MIPs using microfluidics and in situ photo-polymerization. (C) Chemical structures of the target molecule testosterone and its structural analogues β-estradiol and estriol (from left to right).

2 Materials and methods

2.1 Materials

All chemicals and materials were purchased from VWR or Sigma-Aldrich unless stated otherwise. Column chromatography was conducted on silicon dioxide (EcoChrom) and 80 g silica cartridges (Grace Davison Discovery Sciences) using a Büchi automatic column chromatography device. For the fabrication of the microfluidic PDMS stamps, the silicone Sylgard elastomer kit 184 was purchased from Dow Corning Corp, and a 1 mm disposable biopsy punch (Miltex) and Teflon tubes with an outer diameter of 1.17 mm (Alpha Wire) were used. Testosterone, estriol and β-estradiol were purchased from Fluka Analytical. Phosphate buffered saline packs were obtained from Thermo Scientific.

2.2 Synthesis of N,O-bismethacryloyl ethanolamine (NOBE)

For the synthesis of NOBE, a previously reported procedure was followed (Kellens et al. 2016). NOBE was synthesized by mixing 0.450 mol ethanolamine and 0.900 mol triethylamine in dry dimethylformamide with dropwise addition of 1.125 mol methacryloyl chloride under nitrogen at 0 °C. The mixture was stirred for 24 h at 40 °C and afterwards diluted with ethyl acetate. The formed ammonia salts were removed by filtration. All water-soluble contents were extracted by washing with saturated sodium bicarbonate, saturated ammonium chloride, water and saturated sodium chloride aqueous solutions, respectively. The crude product was dried with magnesium sulfate and passed over a basic alumina column to remove residual acids. For the final purification, the product was passed over a silica column using ethyl acetate/petroleum spirit (5/95 ratio) as mobile phase. The monomer yields before and after purification are 85 % and 35 % respectively. Since the monomer is prone to self-polymerization, a significant amount of material is lost during purification. For nuclear magnetic resonance (NMR) data we refer to previously reported results (Kellens et al. 2016).

2.3 Design and Fabrication of Microfluidic Mold

2.3.1 Design and Fabrication of Master Mold

Prior to spin coating, 1 cm x 1 cm silicon substrates (L14016, Siegert Wafer GmbH) were thoroughly cleaned and dehydrated by heating them for 5 min at 150 °C. The negative photoresist SU-8 2025 (Micro Resist Technology GmbH) was diluted by cyclopentanone from a solid-content of 68.6 % to 44.4 %. These solutions were spin coated following manufacturer's specifications and cured for 2 min at 95 °C, resulting in a thick layer of approximately 4.5 µm. The desired pattern of the MIP structures, with specified widths and heights, were designed with the DesignCad lt 2000 software tool. E-beam lithography was performed with a NPGS system (JC Nabity Lithography Systems) mounted on a FEG-SEM (FEI Quanta 200F). The e-beam line-exposure was set at 0.12 nC/cm with an acceleration voltage of 30 kV. After exposure, the SU-8 layers were baked again for 3 min at 110 °C. The substrates were developed with SU-8 developer and rinsed with 2-propanol. The master mold was additionally subjected to a hard-baking step for 2 h at 150 °C to release stress from the resulting SU-8 microstructures and to achieve optimal mechanical stability and durability. The mold can then be reused dozens of times without deteriorating performance.

2.3.2 Design and Fabrication of Microfluidic Stamp

A cast from the master mold was made in PDMS. The base polymer and curing agent were mixed thoroughly in a 10:1 weight-ratio in a disposable recipient. The introduced air from mixing was removed at an absolute pressure of 0.55 bar for at least 30 min. Next, the uncured PDMS was poured over the mold and subsequently baked in an oven for 3 h at 60 °C under normal atmosphere. The resulting PDMS cast of 2.5 mm high was cut out with a scalpel and peeled off from the mold. The inlet and outlet (hereinafter referred to as connection blocks) were punched using a 1 mm biopsy punch and the excess of cured PDMS was removed.

2.3.3 Surface Treatment of NCD Substrates

Highly doped silicon substrates (resistivity 10 – 20 kΩ, p-type doping, 10 mm x 10 mm x 0.525 mm) overgrown with a < 200 nm NCD layer ($[CH_4]/[H_2]$ = 4 %, $[TMB]/[CH_4]$ = 4800 ppm) were cleaned by wet etching for 30 min in an oxidizing mixture of boiling potassium nitrate and sulfuric acid (1:10 ratio), followed by washing in an ultrasonic bath with heated ultrapure water. Next, the substrates were thoroughly rinsed with ultrapure water and dried using nitrogen gas. Hydrogenation of the substrates was performed using an ASTeX® reactor equipped with a 2.45 GHz microwave generator: 2 min at 3500 W, 30 Torr, 500 sccm H_2 and 5 min at 2500 W, 15 Torr, 500 sccm H_2. The substrates were cooled in H_2 atmosphere (500 sccm) for 40 min. Subsequently, a 20 nm thick carbon layer was deposited at 40 amperes onto the H-terminated substrates (Leica EM ACE600, carbon thread evaporation).

2.3.4 Fabrication of Patterned MIP Structures

The formulation used for the fabrication of the MIP structures was achieved by adapting a protocol that was previously published (Kellens et al. 2016), where the affinity and selectivity of the used monomer/target combination and ratio has been studied. The formulation was however optimized to achieve a mixture that can flow through the channels. The tested variations are shown in Table S1. The optimal mixture used comprised of 0.507 mmol NOBE, 0.012 mmol 2,2-dimethoxy-2-phenylacetophenone, 1.088 mmol chloroform and 0.087 mmol testosterone.

The microfluidic stamp was placed onto the freshly carbon coated NCD substrate and Teflon tubes were connected to the inlet and outlet of the stamp. The polymerizable mixture was pumped via the inlet through the microfluidic channels until they were all filled. Next, the tubes were removed and the substrate, with filled microfluidic channels, was placed under UV-light (Lawtronics ME5E UV-lamps, 254 nm, 265 mW/cm^2). The UV-transmittance of PDMS at 254 nm ranges between 40 and 60 % (**Figure S1** in the supplementary information

303 (SI)). Polymerization was done for 20 h in a glovebox under nitrogen environment. After
304 polymerization, the stamp was removed from the substrate.

305 The target molecules were removed from the MIP structures by gently shaking the
306 substrate in a mixture of 1:1 ethanol (EtOH)/ultrapure water (7.5 h, 5x solvent change), a
307 mixture of 1:19 acetic acid/methanol (4 h, 2x solvent change), and a mixture of
308 ethanol/ultrapure water (1 h, 4x solvent change). Non-imprinted polymer structures were
309 synthesized in the absence of the target molecule and washed following the same procedure as
310 for the MIP structures.

311 ***2.4 Characterization of the patterned polymer structures***

312 The integrity of the structures was characterized using an Axiovert 40 MAT optical
313 microscope (Zeiss) equipped with a digital camera and by using the Axiovision AC software.
314 The integrity and geometry of the structures were studied using a scanning electron
315 microscope (SEM, FEI Quanta 200F) operating at an accelerating voltage around 20 kV. The
316 morphology and height of the structures were measured employing the DektakXT
317 profilometer (Bruker).

318 **2.5 *Electrochemical Impedance Spectroscopy (EIS)***

319 The electrochemical testing of the patterned MIP/NIP structures as sensor platform was
320 performed using impedance spectroscopy. The measurements were executed using a custom
321 designed differential impedance sensor-cell set-up (**Figure 3A**), which can measure both MIP
322 and NIP substrates simultaneously, thereby eliminating the influence of the surroundings
323 (such as temperature fluctuations) and sample variations (such as different biological residue
324 content).

325 The flow-through cell has an internal volume of 300 µL and is made of polymethyl
326 methacrylate. All measurements were temperature controlled using a proportional integral
327 derivative controller (P = 5, I = 8, D = 0). The MIP- and NIP-coated electrodes were installed
328 symmetrically with respect to a gold wire serving as a common counter electrode. The contact

area of each electrode with the liquid was defined by O-rings (28 mm²), and the distance from the sensing substrates to the counter electrode was 1.7 mm. Two other (ground) electrodes are present on the copper block of each substrate. The impedance signals were measured in a frequency range of 100 Hz to 100 kHz with 10 frequencies per decade and a scanning speed of 5.69 s per sweep. The amplitude of the alternating current voltage was fixed to 10 mV under open circuit conditions. Silver paste was used to improve the contact between the transducer substrate and the copper blocks.

2.6 Electrochemical Testing of MIP/NIP structures as Sensor Platform

The binding behavior of the MIP and NIP structures for testosterone was tested using EIS at the physiological pH (7.4) and temperature (37 °C). Testosterone solutions were prepared using ethanol/aqueous media mixtures as the former had limited solubility in water. For these experiments, a mix of ethanol and 1x phosphate buffered saline (PBS) solution, filtered urine or saliva (in a 20/80 wt. % ratio, passed through Chromafil filters for polar media, pore size 1 and 5 µm) was spiked with testosterone to obtain the following target molecule concentrations: 0.5, 2, 8, 20, 50, 100, 300 and 500 nM. Subsequently, the sensor substrates were integrated in the differential sensor set-up and the impedance signal was allowed to stabilize in the ethanol/buffer, urine or saliva solution containing no target or analogues molecules (blank sample). After stabilization, 1 mL of the spiked samples was added, from low to high concentration with 15 minutes intervals. To obtain the dose-response graphs, the mean impedance value of the last 35 data points obtained after administration of a certain concentration (Z(t)) was normalized with the initial impedance stabilization value (blank sample, Z(0)). The obtained value was plotted against that specific testosterone concentration. Informed signed consent was obtained from the healthy volunteer who donated urine and saliva. To test the cross-selectivity, impedance measurements were conducted for the structural analogues β-estradiol and estriol using the following concentrations: 0.5, 2, 8, 20, 50 and 100 nM.

3 Results and Discussion

In this work, a patterned MIP structure immobilized on a sensor substrate was realized by combining simple and efficient functionalization of diamond substrates using amorphous carbon coating and patterned microfluidic molds. The bi-functional monomer NOBE was obtained using a previously reported synthesis method (Kellens et al. 2016; LeJeune and Spivak 2007), and testosterone was used as template molecule. The resulting MIP structures were characterized by optical light microscopy, Dektak profilometry and SEM. For the proof-of-concept, the sensor performance was tested using EIS in buffer, urine and saliva spiked with testosterone. The highly stable bonds between the polymer structures and the substrate allowed for successful regeneration of the sensor substrates. The selectivity of the sensor was tested using testosterone structural analogues, namely estriol and *β*-estradiol.

3.1 Fabrication of patterned MIP structures

The new design strategy for the immobilization of MIP structures overcomes the aforementioned disadvantages related to *ex situ* prepared MIP particles and other *in situ* strategies. It includes the direct synthesis of micron-sized MIP structures onto a hydrogen-terminated and carbon-coated (20 nm thick carbon film) nano-crystalline diamond layer on top of highly doped silicon transducer substrates by UV-induced photo-polymerization of vinyl groups, as well as photografting to the carbon layer (**Figure 2**). This process involves few simple sequential steps: initially, carbonaceous material is deposited onto the hydrogen-terminated surface of the diamond transducer element to ensure the subsequent attachment of the MIP structures to the substrate. The role of carbon functionalization is crucial as hydrogen termination of NCD substrates alone for photografting was not sufficient to yield a stable immobilization of the polymer layer (see further text). The integrity of these MIP structures on top of the NCD substrates was checked by Dektak profilometry (SI, **Figure S2 and Figure S3**) and optical microscopy (SI, **Figure S4**). From these analyses, no structural differences

can be observed between MIP and NIP structures. Even after several washing steps the structures were still intact, thereby reflecting the stability of the MIP structures on the substrate. On the contrary, in case of hydrogen termination of NCD substrates without carbon functionalization, the polymerized structures did not survive the washing steps and were detached from the substrate. This control experiment clearly demonstrates the need for the carbon functionalization step prior to polymerization for a stable immobilization of the polymeric structures on the substrate.

Top view and cross-section images of these polymer structures were obtained using SEM (**Figure 2 A - C**). From the cross-section image it can be observed that the polymer structures have a shape resembling the PDMS stamp, however with a reduced dimension as a consequence of polymerization induced shrinkage.

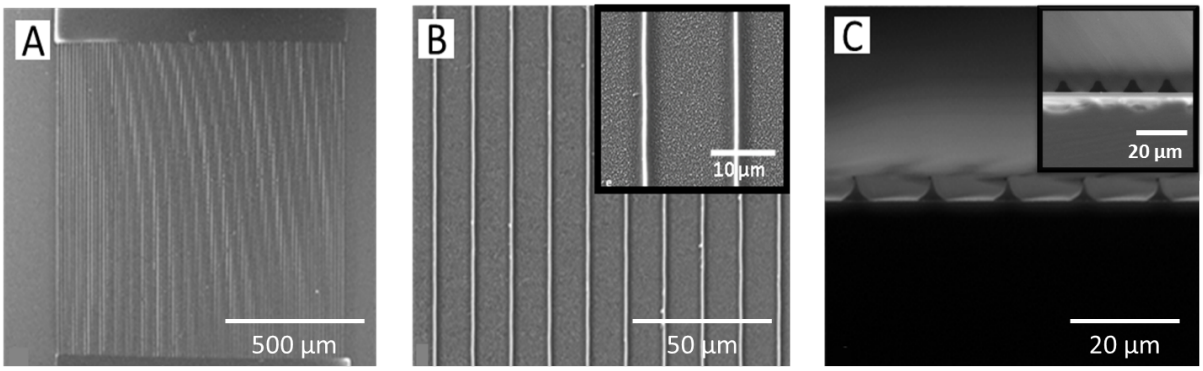

Figure 2. SEM images depicting polymer structures on NCD substrates: (A) Overview illustrating the patterned structure; (B) Top view of structures in higher magnification with the insert showing two lanes in focus, (C) Cross-section view of the polymer structures with the insert showing a cross section of the PDMS stamp.

3.2 Impedimetric testing of patterned MIP structures as sensor platform in buffer solution

As proof-of-concept, the synthesized MIP sensor platform was tested by electronic sensing based on EIS. Both MIP and NIP structures have an identical surface coverage and polymer distribution as they were synthesized using identical PDMS stamps. Therefore, the precondition for differential measurements – having identical surface loadings – was complied.

For the detection using EIS, a custom designed differential set-up was used to measure the binding activity of the MIP and NIP in an identical environment (**Figure 3A**). The flow-through cell was filled with an ethanol/PBS solution (20/80 wt. %) at a pH of 7.4 to simulate a physiological acidity environment. After stabilization at the physiological temperature of 37 °C, 1 mL of increasing known concentrations of testosterone ranging between 0.5 and 500 nM was added stepwise with intervals of 15 minutes. All dose-response curves for testosterone detection in buffer solutions were determined at a frequency of 1,258 Hz. This frequency was chosen because it offered a good signal-to-noise ratio, which resulted in a very stable impedance signal with a small standard deviation of approximately 0.18 %.

The resulting dose-response curves are shown in **Figure 3**. The y-axis represents the normalized impedance change and the x-axis the concentration of administered testosterone. The graphs in **Figure 3** clearly demonstrate that a significant difference exists in sensor response between the MIP and NIP upon increasing target molecule concentration. The binding of testosterone to the polymer causes an increase in the complex resistance. The highest added testosterone concentration (500 nM) resulted in an increase of the impedance signal with 10.03 ± 0.19 % for the MIP and 1.89 ± 0.23 % for the NIP. Even the addition of the lowest testosterone concentration (0.5 nM) led to a measurable increase in the MIP signal of 1.8 ± 0.15 %, which is clearly visible from the plot in the logarithmic scale (**Figure 3B**). This testosterone concentration is situated well within the physiological range of 0.5 – 60 nM (Jin et al. 2007; Taieb et al. 2003). The sensor response of the NIP was comparatively low, indicating only small amounts of aspecific binding of testosterone. The latter is in accordance

with our previous reported studies (Kellens et al. 2016). The increase in the occupation of the MIP binding sites by testosterone leads to a trend toward saturation for concentrations higher than 20 nM. The impedimetric response upon target binding was modeled using an equivalent circuit (SI, **Figure S5 and Table S2**). The change in the impedance signal is attributed to the change in the capacitance at the functionalized electrode interface due to the binding of the testosterone molecules to the MIP cavities. This observation is in accordance to the previous findings (Peeters et al. 2012) where it was described that the binding leads to the replacement of water molecules by the organic molecules (lower dielectric constant as compared to water). Additionally, the effective contact area between the electrode and electrolyte is also affected as more target molecules bind to MIP layer. In our case, as the substrate is a highly doped semiconductor, the electronic properties of the substrate with the MIP functional layer is also influenced by the target molecule binding, while the NIP substrate shows no characteristic change in its electronic properties.

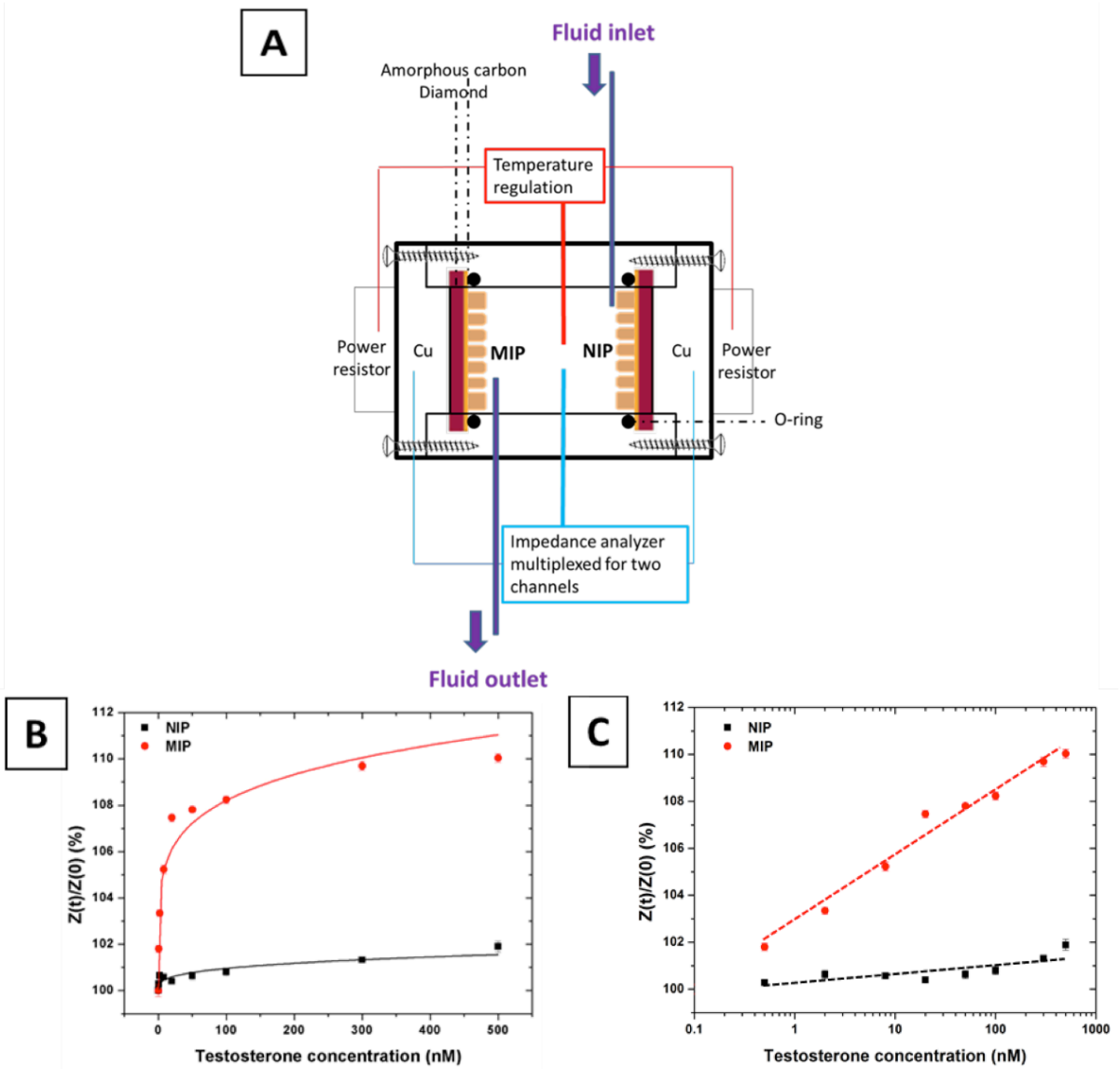

441

442 **Figure 3**. (A) Schematic representation of the differential impedimetric flow cell used for the
443 simultaneous measurements of MIP and NIP substrates; (B) EIS dose-response curves (fitted
444 non-linearly, R^2 = 0.91 for MIP and 0.87 for NIP) of the MIP and NIP structures exposed to
445 increasing concentrations of testosterone in EtOH/PBS buffer solution; (C) Dose-response
446 curves identical to (B) but with the testosterone concentration plotted in logarithmic scale to
447 clearly illustrate the response at the lowest concentrations. The dotted lines serve as a guide to
448 the eye to give an indication about the linear behavior at these concentrations.

449

The obtained result clearly proves that by employing this simple fabrication technique, a sensor platform with well-defined MIP structures is achieved, resulting in sensitive and high performance measurements. In addition, as a proof of concept, the sensor substrate was tested for reusability by washing the bound testosterone molecules. As a proof for regeneration, the substrates that were used to construct **Figure 3** were washed subsequently for a second time with the same solvent mixtures (as explained in the experimental section) to remove bound testosterone from the polymers. The polymer structures remained intact after washing when observed with the optical microscope. A subsequent impedance sensor measurement was performed with these substrates and the resulting dose response curve is shown in **Figure 4**.

From **Figure 4** it can be seen that the MIP structures are still capable of binding a high amount of testosterone in comparison to the NIP structures, even after regeneration. When the highest concentration of testosterone is added (500 nM), the impedance signal increases by (8.40 ± 0.26) % for the MIP and (0.90 ± 0.09) % for the NIP. However, these values are not as high as the values obtained from the previous sensor measurement. This effect can be due to incomplete testosterone removal after the second washing procedure, which can be improved by optimizing the washing protocol.

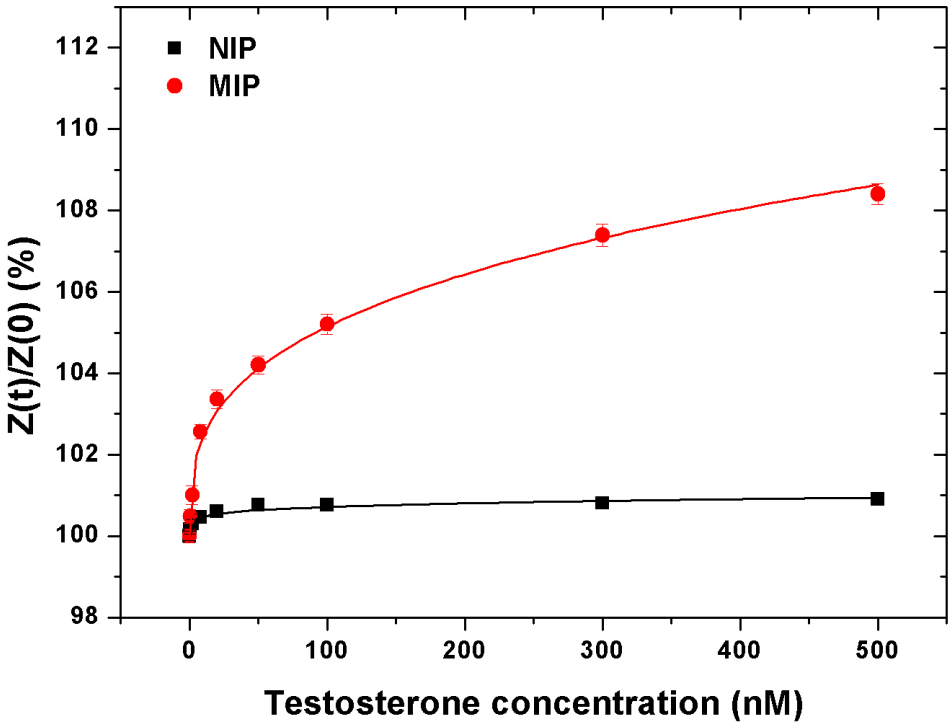

Figure 4: EIS dose-response curves (fitted non-linearly, $R^2 = 0.93$ for NIP and 0.99 for MIP) of the regenerated MIP and NIP substrates.

3.3 Selectivity testing of the senor platform in buffer solution

To test the selectivity of the MIP structures, sensor measurements were performed wherein testosterone was replaced with structurally similar molecules. The obtained dose-response data recorded at a frequency of 1,258 Hz for the MIP and NIP structures exposed to increasing concentrations of estriol and β-estradiol are shown in **Figure 5**.

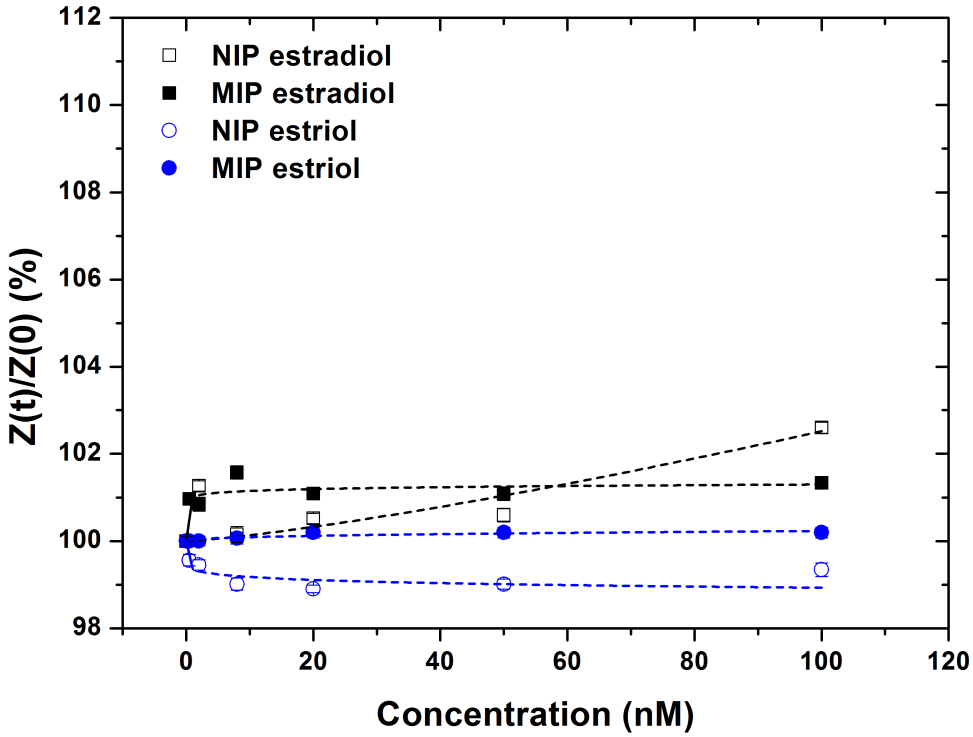

Figure 5. EIS dose-response curves of the MIP and NIP structures exposed to increasing concentrations of estriol and *β*-estradiol in EtOH/PBS buffer solution. The dotted lines serve as a guide to the eye to show the trend of the sensor response.

It can be clearly seen that *β*-estradiol shows some affinity to the MIP structures while estriol shows no specific binding at all. A concentration of 100 nM resulted in an increase of the MIP impedance signal with 0.19 ± 0.12 % for estriol and 2.6 ± 0.12 % for *β*-estradiol. Both estriol and *β*-estradiol are different from testosterone since they both lack the methyl group at the C-19 position and have a hydroxyl group at the C-3 position instead of a ketone. Compared to *β*-estradiol, estriol shows the largest structural variation with testosterone because of its excess hydroxyl group at the C-16 position, which provides steric hindrance during the binding to the testosterone imprints. This explains the low or non-existing affinity between the MIP and estriol. *β*-estradiol, which lacks the C-16 hydroxyl group, shows a small affinity towards the obtained MIPs. However, this is still less pronounced in comparison with

492 the affinity for the template molecule testosterone. These findings are in agreement with our
493 previous report and underpin the high selectivity of the MIPs obtained (Kellens et al. 2016).
494
495 **3.4 Impedimetric testing of the sensor platform in body fluids**
496 After obtaining a selective response from the MIP structures in EtOH/PBS buffer
497 solutions, the same experiments were performed with testosterone-spiked solutions where the
498 PBS buffer was replaced with urine or saliva. These body fluids were obtained from a healthy
499 volunteer and, as a preparation step, they were filtered in order to remove large structures (any
500 residual cells and other large impurities). This way, the binding characteristics of the MIP and
501 NIP structures can be analyzed in the presence of other molecules such as hormones, vitamins,
502 proteins, etc., which are present in real patient samples that can potentially block the imprints.
503 The results obtained with the EtOH/urine solution are shown in **Figure 6**. The optimal
504 frequency – where the highest signal to noise ratio is observed – for the measurements was
505 501 Hz due to the presence of proteins, hormones, or other potentially interfering substances
506 in urine.
507

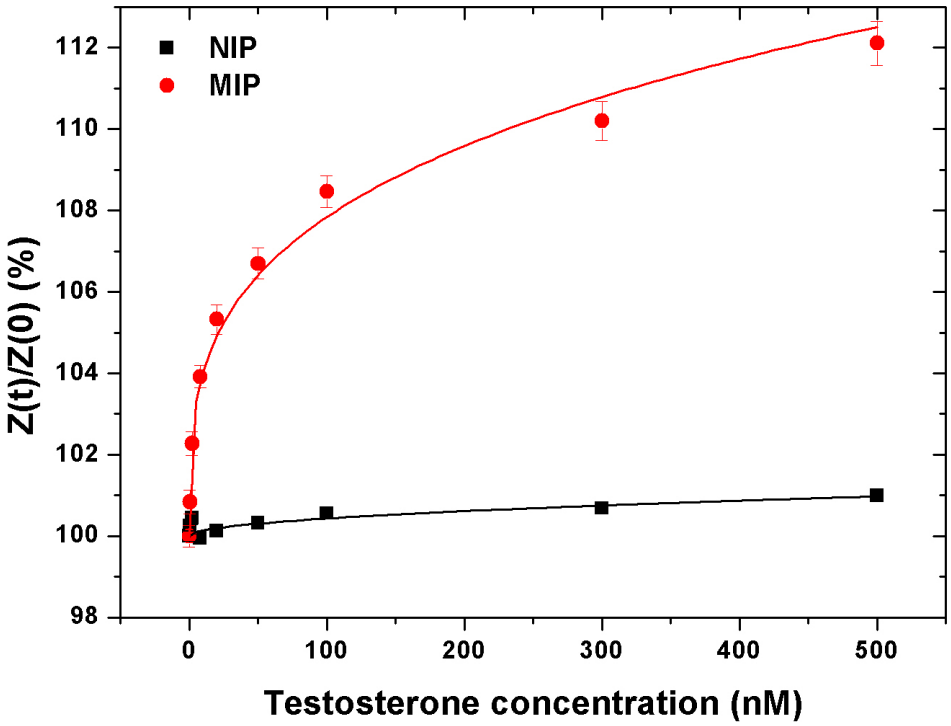

Figure 6. EIS dose-response curve (fitted non-linearly, R^2 = 0.80 for NIP and 0.98 for MIP) of the MIP and NIP structures exposed to increasing concentrations of testosterone in EtOH/urine solution.

The maximum impedance increases of the NIP and MIP after adding a concentration of 500 nM testosterone were (0.99 ± 0.09) % and (12.11 ± 0.53) % respectively. At lower testosterone concentrations of 0.5 and 2 nM, the MIP structures gave a sensor response of (0.84 ± 0.29) % and (2.27 ± 0.29) %, respectively. This limit of detection is in accordance with Batatache *et al.* where they combined MIP film detection with EIS read-out (Betatache et al. 2014). These results show that even in complex samples, the MIP structure is still able to detect testosterone in a specific way.

Also, in saliva-based samples the MIP structures were able to specifically bind testosterone. The obtained results are shown in the supplementary information (**Figure S6**). In saliva, the MIP sensor performance was lower compared to the one obtained in buffer and

523 urine; with a maximum impedance increase of (3.63 ± 0.32) % at 500 nM testosterone. The
524 impedance increase for the NIP at this testosterone concentration is (1.20 ± 0.24) %. This
525 effect can be explained by the fact that there are more proteins and other molecules present in
526 saliva in comparison with buffer and urine which substantially block the testosterone imprints.
527 However, this can in principle be circumvented by pretreating the saliva samples. Regardless,
528 the MIP structures still show a better response than the control NIP structures.

529
530

4 Conclusions

Patterned microstructures of molecularly imprinted polymers on functionalized NCD substrates were created with testosterone as target molecule and NOBE as a bi-functional monomer. A master structure, which was obtained using e-beam lithography, was used to fabricate structured PDMS stamps. The latter were used to obtain patterned polymer structures that were covalently attached to the amorphous carbon coated diamond substrate. The obtained structures were characterized using optical microscopy, SEM and height profilometry. We could demonstrate that the structures remained intact on the substrate even after several washing steps. The affinity and selectivity of these sensor substrates for the target molecule testosterone were tested using EIS as a readout technique. The structured polymers were able to detect testosterone with a detection limit of 0.5 nM and showing saturation at concentrations above 20 nM. The ability to detect small concentrations with high specificity in buffer, urine and saliva samples shows the application potential of these structures. As a proof of concept, it was also shown that the polymer structures could be regenerated after a sensor measurement. This promising result opens new avenues toward reusable MIP based sensors.

It may be concluded that our approach offers a simple and cost-effective method to produce sensitive, high performant, reproducible and well-defined MIP based sensor platforms for the electronic detection of target molecules. The fabrication method offers design flexibility that can be used for tuning the dimensions and amount of MIP structures by opting for suitable master structures, which provide increased active sensing surfaces. The latter, in combination with a miniaturized measuring cell, can eventually lead to achievement of an even lower limit of detection. The microfabrication approach employing microfluidic molds can be extended to deposit multiple structures imprinted with different target molecules on the same substrate using independent stamps in order to realize applications that require multi-analyte sensing.

Acknowledgements

E.K. and H.B. contributed equally to this work. E.K. gratefully acknowledges the financial support by the Agency for Innovation by Science and Technology (IWT). H.B. is an FWO doctoral fellow. K.H. acknowledges the financial support provided by the Methusalem NANO network. The authors also thank additional financial support from UHasselt BOF funds. The authors gratefully acknowledge technical support by B. Ruttens, H. Pellaers, C. Willems, and J. Baccus.

References

Acikgoz, C., Hempenius, M.A., Huskens, J., Vancso, G.J., 2011. Eur. Polym. J. 47(11), 2033-2052.

Alenus, J., Galar, P., Ethirajan, A., Horemans, F., Weustenraed, A., Cleij, T.J., Wagner, P., 2012. Phys. Status Solidi A 209(5), 905-910.

Alexander, C., Andersson, H.S., Andersson, L.I., Ansell, R.J., Kirsch, N., Nicholls, I.A., O'Mahony, J., Whitcombe, M.J., 2006. J. Mol. Recognit. 19(2), 106-180.

Apodaca, D.C., Pernites, R.B., Del Mundo, F.R., Advincula, R.C., 2011. Langmuir 27(11), 6768-6779.

Ayela, C., Dubourg, G., Pellet, C., Haupt, K., 2014. Adv. Mater. 26(33), 5876-5879.

Bakowicz-Mitura, K., Bartosz, G., Mitura, S., 2007. Surf. Coat. Technol. 201(13), 6131-6135.

Betatache, A., Lagarde, F., Sanglar, C., Bonhommé, A., Léonard, D., Jaffrezic-Renault, N., 2014. Sens. Trans. J. 27, 92-99.

Birnbaumer, G.M., Lieberzeit, P.A., Richter, L., Schirhagl, R., Milnera, M., Dickert, F.L., Bailey, A., Ertl, P., 2009. Lab on a Chip 9(24), 3549-3556.

Boysen, R.I., Schwarz, L.J., Li, S., Chowdhury, J., Hearn, M.T., 2014. Microsyst. Technol. 20(10-11), 2037-2043.

Cauley, J.A., Lucas, F.L., Kuller, L.H., Stone, K., Browner, W., Cummings, S.R., 1999. Ann. Intern. med. 130(4), 270-277.

Chen, L., Wang, X., Lu, W., Wu, X., Li, J., 2016. Chem. Soc. Rev. 45(8), 2137-2211.

Chen, Y., Liu, Y., Shen, X., Chang, Z., Tang, L., Dong, W.-F., Li, M., He, J.-J., 2015. Sensors 15(12), 29877.

Chianella, I., Piletsky, S.A., Tothill, I.E., Chen, B., Turner, A.P.F., 2003. Biosens. Bioelectron. 18(2–3), 119-127.

Choi, K.M., 2014. Bio-Chemical Sensors based on Molecularly Imprinted Polymers; Soft Lithography, Microfabrication and Microfluidic Synthesis. One Central Press

Eersels, K., van Grinsven, B., Ethirajan, A., Timmermans, S., Jiménez Monroy, K.L., Bogie, J.F.J., Punniyakoti, S., Vandenryt, T., Hendriks, J.J.A., Cleij, T.J., Daemen, M.J.A.P., Somers, V., De Ceuninck, W., Wagner, P., 2013. ACS Appl. Mater. Interfaces 5(15), 7258-7267.

Fitzgerald, R.L., Griffin, T.L., Herold, D.A., 2010. Methods Mol. Biol. 603, 489-500.

Fuchs, Y., Soppera, O., Mayes, A.G., Haupt, K., 2013. Adv. Mater. 25(4), 566-570.

Gates, B.D., Xu, Q., Love, J.C., Wolfe, D.B., Whitesides, G.M., 2004. Annu. Rev. Mater. Res. 34, 339-372.

Gooding, J.J., 2002. Electroanal. 14(17), 1149-1156.

Grieten, L., Janssens, S., Ethirajan, A., Bon, N.V., Ameloot, M., Michiels, L., Haenen, K., Wagner, P., 2011. Phys. Status Solidi A 208(9), 2093-2098.

Hartl, A., Schmich, E., Garrido, J.A., Hernando, J., Catharino, S.C., Walter, S., Feulner, P., Kromka, A., Steinmuller, D., Stutzmann, M., 2004. Nat. Mater. 3(10), 736-742.

Hernando, J., Pourrostami, T., Garrido, J.A., Williams, O.A., Gruen, D.M., Kromka, A., Steinmüller, D., Stutzmann, M., 2007. Diam. Relat. Mater. 16(1), 138-143.

Hutter, N.A., Steenackers, M., Reitinger, A., Williams, O.A., Garrido, J.A., Jordan, R., 2011. Soft Matter 7(10), 4861-4867.

Hyde, Z., Flicker, L., McCaul, K.A., Almeida, O.P., Hankey, G.J., Chubb, S.P., Yeap, B.B., 2012. Cancer Epidem. Biomar. 21(8), 1319-1329.

Jin, H., Lin, J., Fu, L., Mei, Y.F., Peng, G., Tan, X., Wang, D.M., Wang, W., Li, Y.G., 2007. Biochem. Cell Biol. 85(2), 246-251.

Kamra, T., Chaudhary, S., Xu, C., Johansson, N., Montelius, L., Schnadt, J., Ye, L., 2015. J. Colloid Interface Sci. 445, 277-284.

613 Kellens, E., Bové, H., Conradi, M., D'Olieslaeger, L., Wagner, P., Landfester, K., Junkers, T.,
614 Ethirajan, A., 2016. Macromolecules 49(7), 2559-2567.
615 Lavine, B.K., Westover, D.J., Kaval, N., Mirjankar, N., Oxenford, L., Mwangi, G.K., 2007.
616 Talanta 72(3), 1042-1048.
617 LeJeune, J., Spivak, D.A., 2007. Anal. Bioanal. Chem. 389(2), 433-440.
618 Linares, A.V., Falcimaigne‐Cordin, A., Gheber, L.A., Haupt, K., 2011. Small 7(16), 2318-
619 2325.
620 Liss, M., Petersen, B., Wolf, H., Prohaska, E., 2002. Anal. Chem. 74(17), 4488-4495.
621 Liu, H., Ni, T., Mu, L., Zhang, D., Wang, J., Wang, S., Sun, B., 2018. Sens. Actuator B:
622 Chem. 256, 1038-1044.
623 Peeters, M., Troost, F., van Grinsven, B., Horemans, F., Alenus, J., Murib, M.S., Keszthelyi,
624 D., Ethirajan, A., Thoelen, R., Cleij, T., 2012. Sens. Actuator B: Chem. 171, 602-610.
625 Peeters, M., Troost, F.J., Mingels, R.H., Welsch, T., van Grinsven, B., Vranken, T.,
626 Ingebrandt, S., Thoelen, R., Cleij, T.J., Wagner, P., 2013. Anal Chem 85(3), 1475-1483.
627 Pérez-Moral, N., Mayes, A.G., 2004. Anal. Chim. Acta 504(1), 15-21.
628 Piletsky, S.A., Alcock, S., Turner, A.P.F., 2001. Trends Biotechnol. 19(1), 9-12.
629 Reimhult, K., Yoshimatsu, K., Risveden, K., Chen, S., Ye, L., Krozer, A., 2008. Biosens.
630 Bioelectron. 23(12), 1908-1914.
631 Rubio-Retama, J., Hernando, J., López-Ruiz, B., Härtl, A., Steinmüller, D., Stutzmann, M.,
632 López-Cabarcos, E., Antonio Garrido, J., 2006. Langmuir 22(13), 5837-5842.
633 Ruigrok, V.J., Levisson, M., Eppink, M.H., Smidt, H., van der Oost, J., 2011. Biochem. J.
634 436(1), 1-13.
635 Sellergren, B., 2000. Molecularly Imprinted Polymers. Man-Made Mimics of Antibodies and
636 their Application in Analytical Chemistry. Elsevier Science, Amsterdam, The Netherlands.
637 Sellergren, B., Allender, C., 2005. Adv. Drug Deliv. Rev. 57(12), 1733-1741.
638 Steenackers, M., Jordan, R., Küller, A., Grunze, M., 2009. Adv. Mater. 21(28), 2921-2925.
639 Svenson, J., Nicholls, I.A., 2001. Anal. Chim. Acta 435(1), 19-24.
640 Taieb, J., Mathian, B., Millot, F., Patricot, M.C., Mathieu, E., Queyrel, N., Lacroix, I.,
641 Somma-Delpero, C., Boudou, P., 2003. Clin. Chem. 49(8), 1381-1395.
642 Tan, Y., Jing, L., Ding, Y., Wei, T., 2015. Appl. Surf. Sci. 342, 84-91.
643 Thieme, D., Hemmersbach, P., 2009. Doping in sports. Springer Science & Business Media.
644 Tretjakov, A., Syritski, V., Reut, J., Boroznjak, R., Öpik, A., 2016. Anal. Chim. Acta 902,
645 182-188.
646 Vaihinger, D., Landfester, K., Kräuter, I., Brunner, H., Tovar, G.E.M., 2002. Macromol.
647 Chem. Phys. 203(13), 1965-1973.
648 van Grinsven, B., Vanden Bon, N., Grieten, L., Murib, M., Janssens, S.D., Haenen, K.,
649 Schneider, E., Ingebrandt, S., Schoning, M.J., Vermeeren, V., Ameloot, M., Michiels, L.,
650 Thoelen, R., De Ceuninck, W., Wagner, P., 2011. Lab Chip 11(9), 1656-1663.
651 Vera, F., Zenuto, R.R., Antenucci, C.D., Busso, J.M., Marín, R.H., 2011. J. Exp. Zool. Part A
652 315A(9), 572-583.
653 Vermeeren, V., Grieten, L., Vanden Bon, N., Bijnens, N., Wenmackers, S., Janssens, S.D.,
654 Haenen, K., Wagner, P., Michiels, L., 2011. Sens. Actuator B: Chem. 157(1), 130-138.
655 Wackers, G., Vandenryt, T., Cornelis, P., Kellens, E., Thoelen, R., De Ceuninck, W., Losada-
656 Perez, P., van Grinsven, B., Peeters, M., Wagner, P., 2014. Sensors 14(6), 11016-11030.
657 Wang, J., 2001. Electroanal. 13(12), 983.
658 Wang, Y., Gay, G.D., Botelho, J.C., Caudill, S.P., Vesper, H.W., 2014. Clin. Chim. Acta 436,
659 263-267.
660 Weng, C.-H., Yeh, W.-M., Ho, K.-C., Lee, G.-B., 2007. Sens. Actuator B: Chem. 121(2),
661 576-582.
662 Wenmackers, S., Vermeeren, V., vandeVen, M., Ameloot, M., Bijnens, N., Haenen, K.,
663 Michiels, L., Wagner, P., 2009. Phys. Status Solidi A 206(3), 391-408.

Whitcombe, M., Vulfson, E., 2001. Adv. Mater. 13(7), 467-478.
Wild, D., 2013. The Immunoassay Handbook (Fourth Edition). Elsevier, Oxford.
Yang, M., Gu, W., Sun, L., Zhang, F., Ling, Y., Chu, X., Wang, D., 2010. Talanta 81(1-2), 156-161.
Yang, Q., Li, J., Wang, X., Peng, H., Xiong, H., Chen, L., 2018a. Biosens. Bioelectron.
Yang, Q., Wu, X., Peng, H., Fu, L., Song, X., Li, J., Xiong, H., Chen, L., 2018b. Talanta 176, 595-603.
Yang, W., Auciello, O., Butler, J.E., Cai, W., Carlisle, J.A., Gerbi, J.E., Gruen, D.M., Knickerbocker, T., Lasseter, T.L., Russell, J.N., Jr., Smith, L.M., Hamers, R.J., 2002. Nat. Mater. 1(4), 253-257.